Biochem. J. (1980) **189**, 421–433
Printed in Great Britain

Analysis of progress curves

RATE LAW OF PYRUVATE KINASE TYPE I FROM *ESCHERICHIA COLI*

Mario MARKUS,* Theo PLESSER,* Arnold BOITEUX,* Benno HESS* and Massimo MALCOVATI†
**Max-Planck-Institut für Ernaehrungsphysiologie, 4600 Dortmund 1, Rheinlanddamm 201, Federal Republic of Germany, and †Istituto di Chimica Biologica, Università di Pavia, Via T. Taramelli 1, 27100 Pavia, Italy*

(*Received 15 January 1980*)

Progress curves of the reaction catalysed by pyruvate kinase from *Escherichia coli* K12, designed to cover the four-dimensional concentration space of phosphoenolpyruvate, ADP, Mg^{2+} and ATP in the regulatory region, were recorded with the pH-stat method (pH 7.0 and 25°C). Additional initial-rate measurements were performed to assess specific points. Two methods for the evaluation of progress curves were used: fitting the rate law to the rates obtained from the tangents of the progress curves and fitting the integrated rate law directly to the curves. Two models, both extensions of the concerted model given by Monod, Wyman & Changeux [(1965) *J. Mol. Biol.* **12**, 88–118] with four protomers, could be fitted to the data within the experimental error. Model discrimination in favour of one of these models was possible by proper experimental design. In the selected model one conformational state of the enzyme forms the active complex. The active site of a second conformational state forms abortive complexes with Mg^{2+}, causing strong inhibition at high Mg^{2+} concentrations. In the absence of ligands, most of the enzyme is in a third state that binds ATP at an allosteric site.

In *Escherichia coli* K12 two types of the glycolytic enzyme pyruvate kinase (EC 2.7.1.40) have been identified: type I, which is sensitive to fructose 1,6-bisphosphate, and type II, which is not influenced by fructose 1,6-bisphosphate. Some properties of pyruvate kinase type I have been described (Malcovati & Kornberg, 1969; Waygood & Sanwal, 1972, 1974; Gibriel & Doelle, 1975; Waygood *et al.*, 1976; Boiteux *et al.*, 1976). It is a tetrameric protein with a molecular weight of 240000 and apparently composed of identical monomers (Waygood & Sanwal, 1974). The dependences of the reaction rate on the concentrations of phosphoenolpyruvate, Mg^{2+} and Mn^{2+} are sigmoid. These dependences become hyperbolic on addition of fructose 1,6-bisphosphate. The dependences of the reaction rate on the concentration of ADP are always hyperbolic.

Kinetic investigations on pyruvate kinase I from *E. coli* published up to now were based on experiments designed for only one rate-determining ligand. Moreover, the regulatory role of the catalytically essential ligand Mg^{2+} was not investigated in detail. Hitherto no rate law has been given in the literature for this enzyme.

In what follows, we set up a model implying a rate law that describes quantitatively the kinetics of pyruvate kinase I from *E. coli* for $v > 0.05\,V_{max.}$ in a concentration region [the term 'region' is defined in *Webster's Dictionary* (1964), page 1912; 'a mathematical aggregate consisting of the totality of all values of an aggregate of continuous variables each varying over an interval'] defined by the following constraints: $0 < [\text{phosphoenolpyruvate}_{total}] < 50\,mM$, $0 < [ADP_{total}] < 30\,mM$, $0 < [ATP_{total}] < 30\,mM$, $0.5 < [Mg^{2+}] < 20\,mM$.

Methods and materials

Recording of progress curves

The concentration region was covered by using an automated digital read-out following the progress of the enzymic reaction (Boiteux *et al.*, 1976). Prerequisites for the application of this technique are a pure and stable enzyme and computer facilities for the complex data evaluation involved.

The progress of the reaction is recorded by titration of the protons absorbed in the phosphate transfer according to the equation:

$$ADP^{3-} + \text{phosphoenolpyruvate}^{2-} + 5H^+ \xrightarrow[\text{kinase}]{\text{Pyruvate}} \text{pyruvate} + ATP^{4-} + 4H^+ \quad (1)$$

0306-3275/80/090421-13$01.50/1

Table 1. *Total initial concentrations of the ligands in progress curve experiments*

For details see the text. Abbreviation used (in this and subsequent Tables and Figures): Pyr-*P*, phosphoenolpyruvate.

Exp. no.	[Pyr-P_{total}] (mM)	[ADP_{total}] (mM)	[Mg_{total}] (mM)	[ATP_{total}] (mM)
1	10	25	45	0
2	50	20	45	0
3	30	30	12	0
4	14	12	30	0
5	12	25	10	0
6	25	12	11	0
7	15	12	10	0
8	25	20	45	0
9	8	20	10	0
10	13	8	50	21
11	13	13	50	17
12	20	25	25	20
13	20	25	45	20
14	20	25	35	20

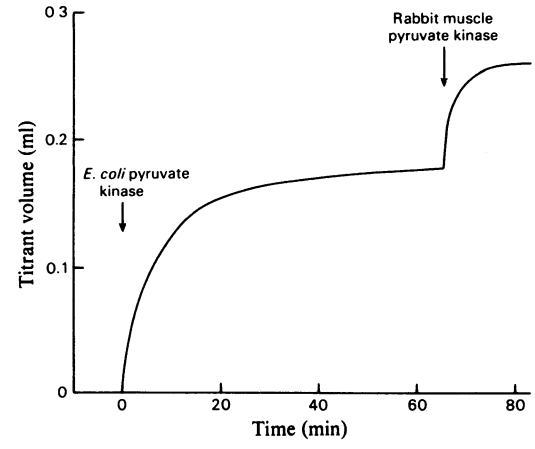

Fig. 1. *Example of a measured progress curve (no. 3 of Table 1)*

Initial conditions: [ADP_{total}] = [Pyr-P_{total}] = 30 mM, [Mg_{total}] = 12 mM, [ATP_{total}] = 0, [E_{total}] = 39.3 nM.

The reaction mixture contained at time zero, in a known volume of approx. 1 ml, 100 mM-KCl and phosphoenolpyruvate, ADP, ATP and $MgCl_2$ at the concentrations given in Table 1. The reaction was started by the addition of 5 μl of pyruvate kinase solution, containing 9.44 μg of enzyme. The resulting enzyme concentration was 39.3 nM. The titrant consisted of 100 mM-HCl and 100 mM-KCl.

All experiments were carried out in a thermostatically controlled reaction vessel at 25°C at pH 7.0 with the titration equipment from Radiometer (Copenhagen, Denmark): Autoburette ABU 13 with digital read-out, titrator TIT60, pH-meter PHM 64, glass electrode G2222 C and a calomel reference glass electrode saturated with KCl. The equipment was coupled to a high-precision digital clock and a computer (Perkin–Elmer 7/32).

The titration steps of the equipment were small enough to compensate for pH changes of 0.001 unit. After each microlitre of titrant consumption, volume data and time were sent to the computer. This step width was sufficient for data collection because the corresponding changes in ligand concentrations were always much smaller than the apparent half-saturation constants. The buffering capacity of the solution due to the binding of protons to substrates and products (no other buffers are present) was included in the calculations; this buffering diminished the pH-stat signal by maximally 10%.

The accuracy of the calibrated burette was better than 0.1%, the time resolution better than 0.01 s. At the end of the progress curve, 2 units (μmol/min) of rabbit muscle pyruvate kinase were added to the assay mixture in order to attain maximal consumption of the limiting substrate (see below under 'Procedures for data evaluation'). Fig. 1 shows, as an example, progress curve no. 3 of Table 1.

Initial-rate measurements

Measurements of initial reaction rates were performed both with the titration technique (for conditions see above) and photometrically. The rate at time zero was determined by the usual graphical method. For optical tests we used a modification of the method of Bücher & Pfleiderer (1955). The standard assay mixture contained (unless otherwise stated) at pH 7.0, in a final volume of 1 ml: 20 mM-Hepes [4-(2-hydroxyethyl)-1-piperazine-ethanesulphonic acid] buffer, 100 mM-KCl, 40 mM-$MgCl_2$, 20 mM-phosphoenolpyruvate, 30 mM-ADP, 0.3 mM-NADH and 11 units (μmol/min) of lactate dehydrogenase (EC 1.1.1.27). The reaction was started by addition of 0.04 μg of pyruvate kinase and followed at 25°C by the decrease in absorbance at 334 nm in a recording spectrophotometer.

Materials

Phosphoenolpyruvate, ADP, ATP, NADH and pig muscle lactate dehydrogenase in 50% glycerol were produced by Boehringer, Mannheim, Germany; all other chemicals were of the highest purity available. Pyruvate kinase I was purified from *E. coli* K12 J53 by the procedure of Malcovati *et al.* (1973).

Procedures for data evaluation

We designate by *S* and *W* the time-dependent concentration of any substrate and the reaction volume respectively. A subscript zero refers to time zero. A measurement takes place at constant pH.

Therefore the following balance equation holds:

$$W_0S_0 = WS + P(W-W_0) + B_0W_0 - BW \qquad (2)$$

The second term on the right-hand side describes the amount of protons titrated into the reaction volume by the titrant with proton concentration *P*. *B* is the time-dependent concentration of protons bound by the substrates and products of reaction (1). Therefore the term B_0W_0-BW takes into account the proton-buffering capacity of the solution.

For our calculations it is important to know the values of the dissociation constants of the cation–product and the cation–substrate complexes. A number of sets of these constants, obtained by different methods, can be taken from the literature for the temperature, the pH and the average ionic strength used in the present work. In order to discriminate among different sets of dissociation constants, we compared the total volume titrated after the addition of rabbit muscle pyruvate kinase at the end of the progress curves with values calculated with the different sets of constants. The total volume depends only on these constants and not on the enzyme. The average of the relative deviation between the measured and the calculated total volume of titrant taken over all progress curves was 0.047 for the selected set in Table 2. A set of constants including the values given by Alberty (1968) yielded a value of 0.069, and a set including the constants given by Langer *et al.* (1977) yielded 0.076. Table 3 shows the abbreviations used for the different ligands. The complexes of K^+ with the phosphate-containing compounds are calculated with the approximation that the concentration of free K^+ can be replaced by the concentration of total potassium.

Rearrangement of eqn. (2) results in:

$$W = W_0 \frac{S_0 + P - B_0}{S + P - B} \qquad (3)$$

Observing that the concentration *S* is a quotient of two time-dependent terms, the amount of substrate

Table 2. *Reactions and dissociation constants used in the calculations*

For details see the text. p*K* is the negative logarithm of the dissociation constant calculated in terms of molar concentrations. Abbreviation: Pyr-*P*, phosphoenolpyruvate.

Reaction	Dissociation constant: Symbol	Value (mM)	p*K*	Reference
$MgPyr\text{-}P^0 \rightleftharpoons Pyr\text{-}P^{2-} + Mg^{2+}$	K_A	5.5	2.26	Wold & Ballou (1957)
$HPyr\text{-}P^- \rightleftharpoons Pyr\text{-}P^{2-} + H^+$	K'_A	4.46×10^{-4}	6.35	Wold & Ballou (1957)
$KPyr\text{-}P^- \rightleftharpoons Pyr\text{-}P^{2-} + K^+$	K''_A	83	1.08	Wold & Ballou (1957)
$MgADP^- \rightleftharpoons ADP^{3-} + Mg^{2+}$	K_B	0.78	3.11	Martell & Schwarzenbach (1956)
$HADP^{2-} \rightleftharpoons ADP^{3-} + H^+$	K'_B	4.5×10^{-4}	6.35	Martell & Schwarzenbach (1956)
$KADP^{2-} \rightleftharpoons ADP^{3-} + K^+$	K''_B	213	0.67	Melchior (1954)
$MgHADP^0 \rightleftharpoons HADP^{2-} + Mg^{2+}$	K'''_B	31.6	1.5	Martell & Schwarzenbach (1956)
$MgATP^{2-} \rightleftharpoons ATP^{4-} + Mg^{2+}$	K_Q	0.1	4.0	Martell & Schwarzenbach (1956)
$HATP^{3-} \rightleftharpoons ATP^{4-} + H^+$	K'_Q	3.16×10^{-4}	6.5	Martell & Schwarzenbach (1956)
$KATP^{3-} \rightleftharpoons ATP^{4-} + K^+$	K''_Q	102	0.99	Melchior (1954)
$MgHATP^- \rightleftharpoons HATP^{3-} + Mg^{2+}$	K'''_Q	10	2.0	Martell & Schwarzenbach (1956)

Table 3. *Abbreviations of the solutes and their concentrations*

Solute	Concentration
Pyr-*P* or A	$[Pyr\text{-}P] = [Pyr\text{-}P^{2-}] + [HPyr\text{-}P^-] + [KPyr\text{-}P^-]$
MgPyr-*P*	$[MgPyr\text{-}P] = [MgPyr\text{-}P^0]$
$Pyr\text{-}P_{total}$	$[Pyr\text{-}P_{total}] = [Pyr\text{-}P^{2-}] + [HPyr\text{-}P^-] + [KPyr\text{-}P^-] + [MgPyr\text{-}P^0]$
ADP or B	$[ADP] = [ADP^{3-}] + [HADP^{2-}] + [KADP^{2-}]$
MgADP	$[MgADP] = [MgADP^-] + [MgHADP^0]$
ADP_{total}	$[ADP_{total}] = [ADP^{3-}] + [HADP^{2-}] + [KADP^{2-}] + [MgADP^-] + [MGHADP^0]$
Mg^{2+} or C	$[Mg^{2+}]$
Mg_{total}	$[Mg_{total}] = [Mg^{2+}] + [MgPyr\text{-}P^0] + [MgADP^-] + [MgHADP^0] + [MgATP^{2-}] + [MgHATP^-]$
ATP or Q	$[ATP] = [ATP^{4-}] + [HATP^{3-}] + [KATP^{3-}]$
MgATP	$[MgATP] = [MgATP^{2-}] + [MgHATP^-]$
ATP_{total}	$[ATP_{total}] = [ATP^{4-}] + [HATP^{3-}] + [KATP^{3-}] + [MgATP^{2-}] + [MgHATP^-]$
K_{total}	$[K_{total}] = [K^+] + [KATP^{3-}] + [KADP^{2-}] + [KPyr\text{-}P^-] \approx [K^+]$

and the volume, differentiation of S with respect to time t reads:

$$\frac{dS}{dt} = -v - \frac{S}{W} \cdot \frac{dW}{dt} \quad (4)$$

where the reaction rate v is defined by the derivative of the product concentration with respect to time at constant volume.

Differentiation of eqn. (3) by using

$$\frac{dB}{dt} = \frac{dB}{dS} \cdot \frac{dS}{dt}$$

and substitution in eqn. (4) results in:

$$\frac{dS}{dt} = -v \frac{S+P-B}{S\frac{dB}{dS}+P-B} \quad (5)$$

For a given rate-law v, the integration of eqn. (5) results in the time course of the substrate concentration S. W then was calculated by using eqn. (3) and fitted to the experimental progress curve.

In the first step of data analysis, where different reaction mechanisms were tested, we fitted the reaction rates obtained at different times from the progress curves. This method is much faster than fitting the titrated volume. We designate the rates obtained from the progress curves by v; they can be calculated with the equation:

$$\tilde{v} = \frac{1}{W} \cdot \frac{dW}{dt} \cdot \frac{S\frac{dB}{dS}+P-B}{1-\frac{dB}{dS}} \quad (6)$$

which results from eqns. (4) and (5) by eliminating dS/dt, solving for v and setting $\tilde{v} = v$. The time derivatives dW/dt of the progress curves were calculated by a spline function approximation (Harwell Subroutine Library, 1973, no. TS01A). The value of S needed in eqn. (6) was obtained by solving iteratively the implicit eqn. (2). B and dB/dS were calculated with the computer by using the constants given in Table 2. Fig. 2 shows, as an example, the rates obtained from the progress curve no. 3 of Table 1 by using eqns. (6) and (2), as described above. $\tilde{v}$ was fitted to the theoretical rate law by using a least-squares procedure for the determination of the unknown parameters (Powell, 1965; Harwell Subroutine Library, 1973, no. VA05A). The natural logarithms of the parameters were optimized. The sum of squares may have several relative minima. To screen for these minima, we performed a large number of independent optimization runs, generating the initial estimates of the parameters by a random-number generator in a parameter region defined by reasonable constraints: turnover numbers between 2×10^2 and $2 \times 10^5 \text{ min}^{-1}$,

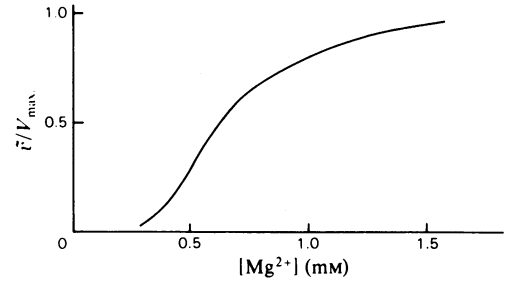

Fig. 2. *Reaction rates obtained from the first derivative of a progress curve*
The reaction rates were normalized with respect to the maximal rate. The derivative was determined from a spline-function approximation of the progress curve no. 3 of Table 1.

dissociation constants between 10^{-3} and 10^5 mM and allosteric constants between 1 and 10^9. The minima were examined more closely with the intention of decreasing the number of parameters as much as possible. If two parameters concerning the same ligand had very similar values after fitting they were set equal, and a new fit was performed; if the sum of squares remained unchanged, we left them equal thereafter. Binding processes with dissociation constants that were much higher than the concentration of the corresponding complex were sequentially left out of consideration if the sum of squares remained unchanged in a new fit of the other parameters.

After fitting the rates obtained from the spline approximation ('differential' method), we refined the parameter determination by fitting the progress curves directly ('integral' method). The numerical integration of eqn. (5) with the rate law (9) was performed with a subroutine from Gear (1971), and for the optimization we used the same procedure as for the fit of the rates.

Experimental error, weighting and enzyme stability

Six replicate measurements of a progress curve with given initial concentrations ($[Mg_{total}] = 20$ mM, $[ADP_{total}] = 20$ mM, $[phosphoenolpyruvate_{total}] = 10$ mM) showed that the errors were approximately proportional to the measured signal (titrant volume), the relative error (standard deviation of the errors divided by the measured signal) being 0.053. The errors of the rates obtained from the tangents of spline-function approximations of the progress curves were seen to be approximately proportional to the square roots of these rates. The differences between these rates and their mean values, divided by the square root of this mean, had a standard deviation of $0.28\sqrt{\text{mM/min}}$. The photometric initial-rate measurements of the present work have an approximately constant relative error of 0.04.

The data were weighted according to our experimental estimations of the error distributions: fits of progress curves and photometric initial-rate measurements were performed by weighting with the reciprocals of the measured signals; fits of rates obtained from progress curves were performed by weighting with the reciprocals of the square roots of the rates.

The best fit of all measured progress curves was consistent with the estimated error distribution: the residuals of the fit were approximately proportional to the square root of the rates when the differential method was used, and approximately proportional to the titrant volume when the integral method was used.

The loss of enzyme activity, being a common source of error, was so low that it could be neglected in the calculations. We could detect no appreciable change in activity of the diluted enzyme during 1 day. A seventh replicate of the progress curve described at the beginning of this section showed deviations comparable with the experimental error after the (undiluted) enzyme had been stored for 9 months.

Stepwise design of experimental conditions

The first seven experiments shown in Table 1 were designed to cover the regulatory region on the basis of the known kinetic properties of the enzyme. The initial concentrations in Expts. 1, 2 and 3 were chosen so that in each case the variation of the concentrations of only one of the ligands phosphoenolpyruvate, ADP and Mg^{2+} affects the rate during the progress of the reaction, whereas the variations of the concentrations of the other ligands are ineffective, since they remain well above their K_m values. In Expts. 4, 5 and 6 the variations of the concentrations of two of the ligands affect the rate: phosphoenolpyruvate and ADP in Expt. 4, phosphoenolpyruvate and Mg^{2+} in Expt. 5 and ADP and Mg^{2+} in Expt. 6. In Expt. 7 the variations of the concentrations of all ligands affect the rate. ATP accumulates in all experiments, starting from zero concentration.

Expts. 1–7 could be fitted within the experimental error by a model published previously (Boiteux *et al.*, 1976). This model had been obtained as an extension of the concerted model given by Monod *et al.* (1965) by assuming random binding of the substrates, two conformational states and binding of Mg^{2+} and ATP at an allosteric site. In order to decrease the errors and the correlation coefficients of the model parameters (e.g. turnover numbers and intrinsic binding constants), we designed Expts. 8–14 of Table 1. Instead of the rough procedure for planning Expts. 1–7, we designed Expts. 8–14 with the more effective D-optimality method (Fedorov, 1972; Markus & Plesser, 1976). Since the model given by Boiteux *et al.* (1976) failed to fit all the 14 progress curves within experimental error, we fitted the more general model given in the Appendix of the present paper, and obtained two different rate laws corresponding to two different minima of the sum of squares with the same depth. For optimal discrimination between the two models we made a new design by using the method of Mannervik (1975), yielding a set of initial-rate experiments.

The model selected by this discrimination was then used for a final design. This design showed that additional kinetic measurements in the given concentration region would be ineffective to further decrease errors and correlations of the model parameters.

Model

The model is based on the assumption that the enzyme consists of four protomers (Waygood & Sanwal, 1974) and that the conformational transitions are concerted. In the time scale observed (we found no lag time within the resolution of the instrument) the rates do not depend explicitly on time and are functions of the ligand concentrations only. (An example out of a series of experiments is shown in Fig. 3.) We assume that all enzyme species are in quasi-equilibrium. The steady-state assumption, being more general, was discarded, because it would imply a substantially larger number of parameters. Furthermore there is hitherto no observation on *E. coli* pyruvate kinase that would be in contradiction with the quasi-equilibrium hypothesis.

For each protomer and each of its conformational states we assumed a general binding scheme, as given in Fig. 4. Random binding of Mg^{2+},

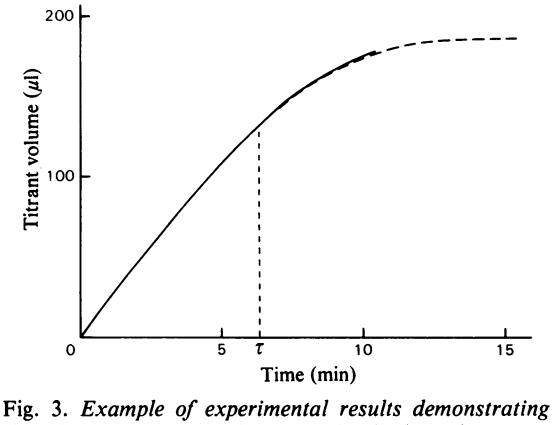

Fig. 3. *Example of experimental results demonstrating that the reaction rates do not explicitly depend on time, but are functions of the ligand concentrations only*
The two progress curves overlap in a common subset of the concentration region although started at different times (time 0 and time τ).

Mg^{2+}-free ADP, Mg^{2+}-free phosphoenolpyruvate and the consideration of ATP as a competitive inhibitor in this scheme is based on investigations by Macfarlane & Ainsworth (1972, 1974) and Ainsworth & Macfarlane (1973). We also considered an allosteric site binding ATP (Johannes & Hess, 1973; Waygood *et al.*, 1976) and Mg^{2+}. The binding scheme in Fig. 4 shows an enzyme–ligand complex in each vertex. The binding of Mg^{2+}-free ligands is represented by the continuous lines and the binding of Mg^{2+} complexes of ligands by the broken lines. The dissociation constants describe the equilibria between the corresponding vertices. The indices A, B, C and Q refer to phosphoenolpyruvate, ADP, Mg^{2+} and ATP respectively, and are written in the order of binding of the ligands to the enzyme. Two indices in parentheses indicate binding of the complex formed by the ligands corresponding to these indices. The last index distinguishes between four conformational states, which we call R_ν ($\nu = 1$, 2, 3, 4). A bar on a dissociation constant (i.e. $\bar{K}$) indicates binding at an allosteric site. Each conformational state was assumed to have a different turnover k_ν. The allosteric constants are defined as $L_\nu = [R_\nu]_F/[R_1]_F (\nu = 2, 3, 4)$, where $[R_\nu]_F (\nu = 1, 2, 3, 4)$ are the concentrations of the states in a ligand-free solution. The dissociation constants of ADP were assumed to be independent of the conformational state because the kinetics of ADP are hyperbolic. The explicit formula of the rate law is given in the Appendix.

The ionic strength I of the reaction medium affects the enzyme so that the percentage increase of I is approximately proportional to the percentage decrease of the enzymic reaction rate, i.e.:

$$\frac{dv(I)}{v(I)} = -z\frac{dI}{I} \tag{7}$$

z is a constant. Integration of eqn. (7) leads to:

$$v(I) = v(\tilde{I})\left(\frac{\tilde{I}}{I}\right)^z \tag{8}$$

where $\tilde{I}$ is a fixed ionic strength, which we set to

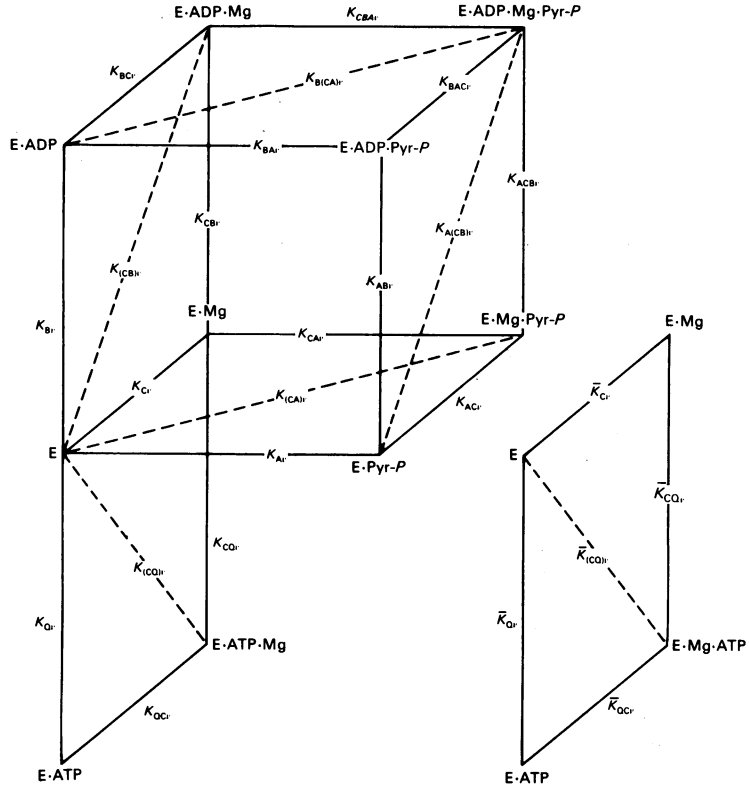

Fig. 4. *General binding scheme considered before optimization*

The enzyme–ligand complexes and the dissociation constants are shown at the vertices and at the edges respectively. Binding processes take place at the active site (dissociation constants K) or at an allosteric site (dissociation constants $\bar{K}$ depicted at the lower right).

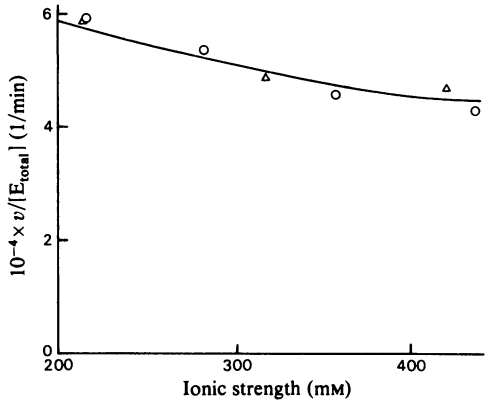

Fig. 5. *Dependence of the reaction rate on ionic strength*
The rates have been normalized with respect to the enzyme concentration. The experiments were performed under conditions of saturation with essential ligands: [Pyr-P_{total}] = 15 mM, [ADP_{total}] = 10 mM, [Mg^{2+}] = 5 mM. The ionic strength was changed by varying the concentration of KCl (△) and that of ATP (○).

300 mM. In order to determine z, the ionic strength I was changed by varying the concentration of KCl in one series of experiments and of ATP in another; the initial rate of the enzymic reaction was determined at each ionic strength by the pH-stat method under conditions of saturation with essential ligands. Under these conditions, $v(\tilde{I})$ is equal to the maximum reaction rate at the fixed ionic strength $\tilde{I} = 300$ mM. The results are shown in Fig. 5. The experimental points obtained with KCl as well as with ATP were fitted by eqn. (8) with 4% accuracy, yielding $z = 0.35 \pm 0.07$. Since the dissociation constants of solutes generally depend on the ionic strength of the solution, a prohibitive number of unknown parameter values should be considered for all chemical species involved. However, the effect of ionic strength is small (see Fig. 5), and it was found sufficient to consider only the empirical overall law given by eqn. (8).

Results

The reaction rates obtained from the progress curves were fitted for the determination of the unknown parameters by using the rate law given in the Appendix corrected for the ionic-strength effects in accordance with eqn. (8). z was set to 0.35. A total of 200 optimization runs were performed with randomly chosen initial estimates for the parameters. In 115 cases the initial estimates were such that the optimization routine found no direction to minimize the sum of weighted squares. In the remaining 85 runs we found the following number of occurrences of standard deviations of the weighted residuals: 27 times, $1.4\sqrt{\text{mM/min}}$; 45 times, $0.61\sqrt{\text{mM/min}}$; 13 times, $0.24\sqrt{\text{mM/min}}$.

Only the standard deviation of $0.24\sqrt{\text{mM/min}}$ is comparable with the error of the data. The 13 fits with this standard deviation correspond to two minima of the same depth. The binding pathways of these two rival models are shown in Fig. 6: model I (broken lines) and model II (continuous lines). The two binding schemes differ as follows: (1) only three states (R_1, R_2 and R_3) appear in model II, whereas all the four states appear in model I; (2) MgADP binds to E only in the conformational state R_2 in model II, whereas it binds to E in all conformational states in model I; (3) only the active site of E in the R_2 state binds Mg^{2+} in model II, whereas only the allosteric site of the states R_1 and R_4 binds Mg^{2+} in model I.

Model discrimination and fit of progress curves

We found only one hint from the literature that would allow us to discriminate between models I and II. The dissociation constant K_{A1} for the binding of phosphoenolpyruvate to the ligand-free enzyme is 0.029 ± 0.015 mM as obtained from our fit with model I, and 0.31 ± 0.18 mM as obtained from our fit with model II; Waygood *et al.* (1976) derived the value 0.17 ± 0.08 mM from binding measurements. Although this could make us decide in favour of model II, we did a discrimination experiment, because the different conditions in the experiments of Waygood *et al.* (1976) may alter the value of K_{A1}. Inspection of Fig. 6 shows that binding of Mg^{2+} on state R_2 causes an inhibition at high Mg^{2+} concentrations for both models. The possibility of direct binding of Mg^{2+} in model II predicts stronger Mg^{2+} inhibition at low ADP concentrations. We looked with the help of the computer for conditions where the difference between the function $v([Mg^{2+}])$ predicted by the two models had its maximum (Mannervik, 1975). Fig. 7 shows the result of photometric initial-rate measurements and the predicted curve before fitting these measurements for model I (broken line) and model II (continuous line). These rate measurements were fitted together with the progress curves. The point corresponding to [Mg_{total}] = 80 mM (outside the investigated concentration region) was not fitted. The average of the weighted residuals for the initial-rate measurements after the fit was 0.22 for model I and 0.051 for model II. Only model II thus gives a fit within the experimental error. Therefore model II is the resulting model within the assumptions given under 'Model' in the Methods and Materials section. Fig. 8 shows the complete set of the experiments and the fit with model II. For this model we found that the dissociation constants of Mg^{2+} after and before the

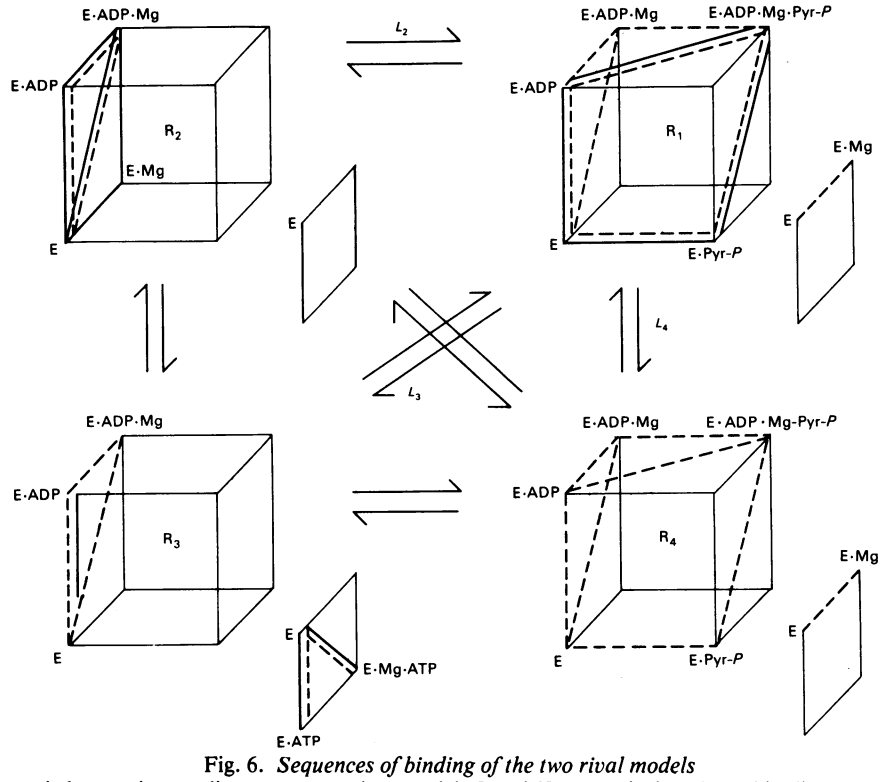

Fig. 6. *Sequences of binding of the two rival models*
The broken and the continuous lines correspond to models I and II respectively. The cubic diagrams illustrate the binding at the active site. The rectangles at the lower right of the cubes illustrate the binding at an allosteric site. Transitions were assumed to be concerted, i.e. the four protomers are all in the state R_1 or all in the state R_2 or all in the state R_3 or all in the state R_4.

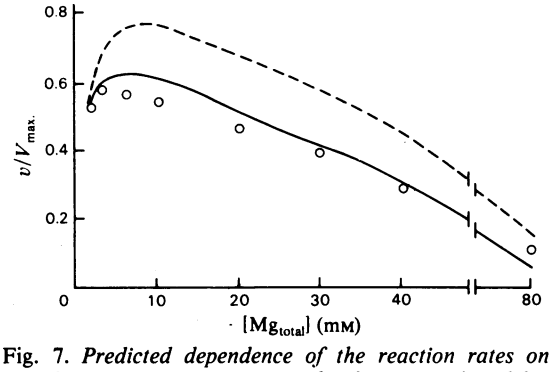

Fig. 7. *Predicted dependence of the reaction rates on total magnesium concentration for the two rival models*
Conditions were chosen such that model discrimination would be optimal: $[ADP_{total}] = 2$ mM, $[Pyr\text{-}P_{total}] = 8$ mM. The broken and the continuous lines correspond to the models I and II respectively. The circles show the experimental points.

binding of ADP at the R_2 state could be set equal without altering the sum of squares, i.e. $K_{BC2} = K_{C2}$. Also, we found that the dissociation constants for binding at an allosteric site of ATP and MgATP can be set equal (i.e. $\bar{K}_{Q3} = \bar{K}_{(CQ)3}$), so that we can describe the inhibition by considering only one binding process, namely the binding of ATP_{total} with a dissociation constant $\bar{K}_{Q3}$.

The rate law for the selected model is given by:

$$v = [E_{total}]\left(\frac{\bar{I}}{I}\right)^z \frac{k_1 \alpha \beta' G_1^3}{G_1^4 + L_2 G_2^4 + L_3 G_3^4} \qquad (9)$$

where $G_1 = 1 + \alpha(1 + \beta') + \beta$, $G_2 = 1 + \beta(1 + \gamma) + \gamma$, $G_3 = (1 + \beta)(1 + \delta)$, $\alpha = [\text{Pyr-}P]/K_{A1}$, $\beta = [ADP]/K_{B1}$, $\beta' = [MgADP]/K_{A(CB)1}$, $\gamma = [Mg^{2+}]/K_{C2}$, $\delta = [ATP_{total}]/\bar{K}_{Q3}$, $K_{A(CB)1}$ is the dissociation constant of MgADP after binding of phosphoenolpyruvate on the state R_1 and is given by $K_{A(CB)1} = K_{AC1}/K_B$, and $[E_{total}]$ is the total enzyme concentration.

Only the points shown by circles in Fig. 8 were evaluated in the optimization, because of limitations in computer capacity. These points were chosen by the D-optimality criterium as described by Markus & Plesser (1976). The best parameter set in the least-square sense corresponds to a standard devia-

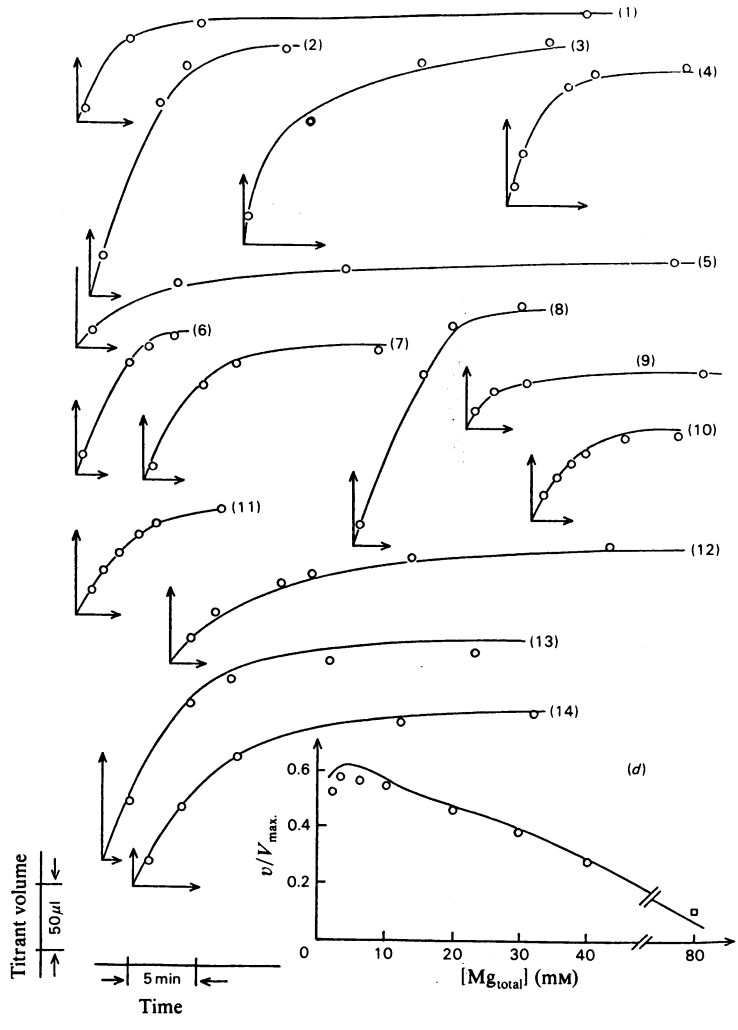

Fig. 8. *Fit of progress curves and discrimination experiments*
The theoretical curves are given by continuous lines and the evaluated experimental points by circles. (1)–(14) Progress curves with initial concentrations as given in Table 1. (*d*) Discrimination experiments (□, not fitted).

tion of weighted residuals equal to 0.049. During the optimization procedure K_{C2} and L_2 were correlated in such a way that only $K_{C2}/\sqrt[4]{L_2}$ was well defined. The final parameters and their correlation coefficients are shown in Table 4. The parameters are well comparable with values given in the literature. The correlation coefficients show low parameter redundancy.

Properties of the model

The model presented here involves concerted transitions between tetramers with conformational states R_1, R_2 and R_3. It is noteworthy that such a three-state model has also been proposed by Minton & Imai (1974) for haemoglobin.

The catalytic active complex of *E. coli* pyruvate kinase is formed only by one conformational state of the enzyme, state R_1 (Fig. 6). This state binds randomly the Mg^{2+}-free ligands ADP or phosphoenolpyruvate. Thereafter the active enzyme complex is formed by binding Mg–phosphoenolpyruvate or MgADP respectively. It is interesting to compare these results with the binding sequences obtained for other enzymes. Balinsky *et al.* (1972) found that pyruvate kinases from normal human liver and from human hepatoma tissue bind phosphoenolpyruvate before ADP. Macfarlane & Ains-

Table 4. *Final parameters of the selected model*

No.	Parameters	Value	Dimension	Remarks
1	k_1	$(5.1 \pm 0.2) \times 10^4$	min^{-1}	$k_1[E_{total}]$ is the maximal rate $V_{max.}$
2	z	0.315 ± 0.006	—	Fit to independent photometric data (Fig. 5) led to $\beta = 0.35 \pm 0.07$
3	$\bar{K}_{Q3}$	22.4 ± 2.1	mM	
4	$K_{C2}/\sqrt[4]{L_2}$	0.59 ± 0.19	mM	
5	K_{B1}	0.18 ± 0.05	mM	
6	K_{A1}	0.31 ± 0.18	mM	K_{A1} is the dissociation constant for the complex formed by Pyr-*P* and the free enzyme; 0.17 mM reported by Waygood *et al.* (1976) at [KCl] = 0
7	$K_{A(CB)1}$	0.44 ± 0.25	mM	$K_{A(CB)1} = K_m$ for MgADP binding to E–Pyr-*P* when all of E is in the state R_1; approximately comparable with: 0.286 mM reported by Gibriel & Doelle (1975); 0.24 mM reported by Waygood & Sanwal (1974)
8	L_3	$(1.15 \pm 0.7) \times 10^3$		
	$\frac{K_{A1}K_{A(CB)1}K_B}{K_{B1}K_A}$	0.11	mM	This quantity is equal to $K_{B(CA)1} = K_m$ for MgPyr-*P* binding to E–ADP when all of E is in the state R_1; approximately comparable with: 0.117 mM reported by Gibriel & Doelle (1975); 0.13 mM reported by Malcovati & Kornberg (1969); 0.03 mM reported by Waygood & Sanwal (1974)

Correlation matrix

These are the correlation coefficients of the logarithms of the parameters

2	−0.34	1					
3	−0.07	0.10	1				
4	0.17	−0.36	0.07	1			
5	0.38	−0.36	−0.15	0.07	1		
6	−0.11	0.33	0.15	0.64	−0.05	1	
7	0.44	−0.78	−0.18	−0.05	0.47	−0.74	1
8	−0.18	0.32	0.00	0.93	0.22	−0.57	0.10
	1	2	3	4	5	6	7

worth (1974) found two possible binding sequences for the fructose 1,6-bisphosphate-activated pig liver pyruvate kinase, both with ADP binding last. Macfarlane & Ainsworth (1972) had earlier found that the reaction mechanism in fructose 1,6-bisphosphate-activated pyruvate kinase from baker's yeast is of the Ordered Tri Bi type with binding in the order phosphoenolpyruvate, ADP and Mg^{2+}. For rabbit muscle pyruvate kinase Ainsworth & Macfarlane (1973) found that the mechanism is not ordered, but of the Random Tri Bi type.

State R_2 of *E. coli* pyruvate kinase binds randomly ADP and Mg^{2+}. It is the only state in which Mg^{2+} can bind to the free enzyme. In the baker's-yeast enzyme (see above) also no binding of Mg^{2+} is possible at the free enzyme in the active conformational state. Our result, that Mg^{2+} is not necessary for the binding of ADP, phosphoenolpyruvate and ATP, is consistent with the binding experiments on *E. coli* pyruvate kinase by Waygood *et al.* (1976) and in disagreement with Cleland's (1967) generalization that nucleoside di- and tri-phosphates bind in the form of their complexes with bivalent metal ions.

Mg^{2+} can inhibit either by binding to the state R_2 or by lowering the concentration of Mg^{2+}-free ADP and phosphoenolpyruvate through complex-formation.

The binding of MgADP after the binding of phosphoenolpyruvate is possible in state R_1 but not in the other states. We should thus expect that under some conditions sigmoidal dependence of the reaction rate on the concentration of ADP should be observed. Simulations with our model showed that such sigmoidicity can appear only at conditions such that $v/V_{max.} < 0.05$, where our model might no longer be valid.

ATP inhibits by virtue of three effects: increase in ionic strength, complex-formation with Mg^{2+} when this metal ion acts as an activator, and binding to the state R_3. However, when conditions are such that Mg^{2+} is an inhibitor, then ATP is expected to activate because of complex-formation with Mg^{2+}. Fig. 9 shows a peak of enzymic activity for the dependence on ATP, as predicted by our model and as measured by photometric initial-rate determinations. The theoretical curve shown in Fig. 8 is especially sensitive to the numerical values of the dissociation constants of the complexes formed by the ligands and Mg^{2+}; the errors in these constants,

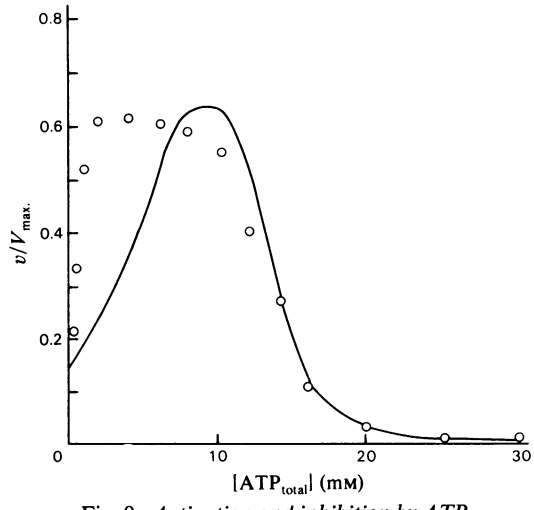

Fig. 9. *Activation and inhibition by ATP*
The continuous lines and the circles show the model prediction and the initial-rate measurements respectively. $[ADP_{total}] = 2$ mM, $[Pyr\text{-}P_{total}] = 3$ mM, $[Mg_{total}] = 17.5$ mM.

as well as their dependence on ionic strength, can thus account for the observed deviation between simulation and experiments. In general, one can say that the ligands Mg^{2+} and ATP cannot be classified as inhibitors or activators, because their regulatory effect on the reaction rate depends on the concentrations of the other ligands.

Competitive inhibition by the product ATP can be neglected. This result is different from that obtained for fructose 1,6-bisphosphate-activated pyruvate kinase from baker's yeast by Macfarlane & Ainsworth (1972), who found that the binding of MgATP and pyruvate at the active site must be considered in their kinetic model. If in our model we replace the binding of ATP at an allosteric site by competitive inhibition, the sum of weighted squares after a new fit is enhanced 4.6-fold. In an earlier report (Boiteux *et al.*, 1979) we had suggested a model that is identical with the model presented here with the exception that the inhibition by ATP is explained by the binding of ATP at an allosteric site on a fourth state. The values of the parameters (except those concerning ATP) and the sum of squares are comparable for both models. We have not been able to design any experiment to discriminate among them. We have chosen here the simpler model.

Furthermore, there is an open question concerning the assumption of quasi-equilibrium. Macfarlane & Ainsworth (1972, 1974) and Ainsworth & Macfarlane (1973) could satisfactorily describe other pyruvate kinases at pH 6.2 by using this assumption. Dann & Britton (1978), however, performed flux-rate and isotope-trapping measurements and found deviations from quasi-equilibrium when phosphoenolpyruvate adds to rabbit muscle pyruvate kinase before ADP. Their experiments were performed at pH 8.5, a condition that is not applicable to our analysis.

In an attempt to identify the proposed conformational states R_1, R_2 and R_3, we analysed the protein fluorescence-intensity spectrum, and found fluorescence quenching on addition of fructose 1,6-bisphosphate as well as by independent addition of Mg^{2+} (A. Boiteux & B. Hess, unpublished work). The quenching effect of fructose 1,6-bisphosphate confirms earlier observations with the enzyme isolated from yeast (Hess *et al.*, 1971). Binding of phosphoenolpyruvate was also identified by fluorescence quenching. For technical reasons we were not able, however, to show experimentally a specific interaction of ATP with the enzyme.

Conclusions

A large number of initial-rate measurements has been performed by several authors to derive rate laws of pyruvate kinase from other sources (Macfarlane & Ainsworth, 1972, 1974; Ainsworth & Macfarlane, 1973; Johannes & Hess, 1973). The analysis of the mechanism of *E. coli* pyruvate kinase given in the present paper, being more complicated than the mechanisms interpreted by these other authors, would imply a discouraging number of initial-rate measurements. Here we showed that experimentation time can be saved by well-designed progress curves. Complementary initial-rate experiments are useful for the investigation of some special aspects of enzyme action.

In the approach used in the present study we made several assumptions, yielding our model. These assumptions either were experimentally justified (such as the assumption of four protomers) or they represent a necessary simplification of the real phenomena (such as our description of the ionic-strength effects) or they represent a choice from several alternative possibilities found in the literature for this enzyme or other pyruvate kinases (such as the assumptions of quasi-equilibrium and of concerted transitions between conformational states). The properties of the model obtained here are only correct in the context of these assumptions made *a priori*. Some variation of the parameters of the model might arise from the choice of the dissociation constants in Table 2. However, with the complementary analysis of fluorescence experiments, the model is significant and its general applicability is supported by the following findings: (1) by including only one more parameter in the model (to take into account exclusive binding of

fructose 1,6-bisphosphate at an allosteric site of the conformation state R_1) 15 additional progress curves with fructose 1,6-bisphosphate could be fitted within experimental error simultaneously with the curves in Fig. 8 (A. Boiteux, M. Markus, Th. Plesser, B. Hess & M. Malcovati, unpublished work); (2) initial-rate measurements showing activation and inhibition by Ca^{2+} can be described by the present model, assuming that Ca^{2+} has the same binding properties as Mg^{2+} but makes turnover impossible (A. Boiteux, M. Markus, Th. Plesser, B. Hess & M. Malcovati, unpublished work); (3) the activity peak for ATP (Fig. 9), which was measured after a prediction with our model, is in accord with an observation by Haeckel *et al.* (1968) on pyruvate kinase from brewer's yeast.

In addition, a model involving two conformational states having similar properties as the states R_1 and R_3 of *E. coli* pyruvate kinase could be fitted to kinetic experiments with the brewer's-yeast enzyme (Boiteux *et al.*, 1979). These experiments extended the experimental range covered by Johannes & Hess (1973).

We thank Dr. H.-J. Wieker for many helpful suggestions during the modelling of the enzyme mechanism and Mr. H. Schlueter for building the electronic reading device of time and volume data. We also thank Mr. E. Hickl for valuable help in the laboratory and Mr. K. Dreher for interfacing the experimental equipment to the computer and for programming assistance.

References

Ainsworth, S. & Macfarlane, N. (1973) *Biochem. J.* **131**, 223–236

Alberty, R. A. (1968) *J. Biol. Chem.* **243**, 1337–1343

Balinsky, D., Cayanis, E. & Bersohn, I. (1972) *Biochemistry* **12**, 863–870

Boiteux, A., Hess, B., Malcovati, M., Markus, M. & Plesser, Th. (1976) *Abstr. Int. Congr. Biochem., Hamburg*, Abstr. 07-4-101

Boiteux, A., Doster, W., Hess, B., Markus, M., Plesser, Th. & Wieker, H.-J. (1979) *Proc. FEBS Meet. 12th, Dresden*, 35–43

Bücher, Th. & Pfleiderer, G. (1955) *Methods Enzymol.* **1**, 435–440

Cleland, W. W. (1967) *Annu. Rev. Biochem.* **36**, 77–112

Dann. L. G. & Britton, H. G. (1978) *Biochem. J.* **169**, 39–54

Fedorov, V. V. (1972) *Theory of Optimal Experiments*, pp. 171–183, Academic Press, New York and London

Gear, C. W. (1971) *Numerical Initial Value Problems in Ordinary Differential Equations*, pp. 158–166, Prentice–Hall, Engelwood Cliffs

Gibriel, A. Y. & Doelle, H. W. (1975) *Microbios* **12**, 179–197

Haeckel, R., Hess, B., Lauterborn, W. & Wuester, K. H. (1968) *Hoppe-Seyler's Z. Physiol. Chem.* **349**, 699–714

Harwell Subroutine Library (1973) *A Catalogue of Subroutines*, Theoretical Physics Division, A.E.R.E., Harwell

Hess, B., Johannes, K.-J., Kutzbach, C., Bishofberger, H.-P., Barwell, C.-J. & Roeschlau, P. (1971) in *Mechanism and Control Properties of Phosphotransferases (Joint Biochemical Symposium USSR–GDR, Schloss Reinhardsbrunn)* (Hofmann, E., ed.), pp. 485–504, Akademie-Verlag, Berlin

Johannes, K. J. & Hess, B. (1973) *J. Mol. Biol.* **76**, 181–205

Langer, R. S., Gardner, C. R., Hamilton, B. K. & Colton, C. K. (1977) *AIChE J.* **23**, 1–10

Macfarlane, N. & Ainsworth, S. (1972) *Biochem. J.* **129**, 1035–1047

Macfarlane, N. & Ainsworth, S. (1974) *Biochem. J.* **139**, 499–508

Malcovati, M. & Kornberg, H. L. (1969) *Biochim. Biophys. Acta* **178**, 420–423

Malcovati, M., Valentini, G. & Kornberg, H. L. (1973) *Acta Vitaminol. Enzymol.* **27**, 96–111

Mannervik, B. (1975) *Biosystems* **7**, 101–119

Markus, M. & Plesser, Th. (1976) *Biochem. Soc. Trans.* **4**, 361–364

Martell, A. E. & Schwarzenbach, S. (1956) *Helv. Chim. Acta* **39**, 653–661

Melchior, N. C. (1954) *J. Biol. Chem.* **208**, 615–627

Minton, A. P. & Imai, K. (1974) *Proc. Natl. Acad. Sci. U.S.A.* **71**, 1418–1421

Monod, J., Wyman, J. & Changeaux, J.-P. (1965) *J. Mol. Biol.* **12**, 88–118

Powell, M. J. D (1965) *Comput. J.* **7**, 303–307

Waygood, E. B. & Sanwal, B. D. (1972) *Biochem. Biophys. Res. Commun.* **48**, 402–407

Waygood, E. B. & Sanwal, B. D. (1974) *J. Biol. Chem.* **249**, 265–274

Waygood, E. B., Mort, J. S. & Sanwal, B. D. (1976) *Biochemistry* **15**, 277–282

Wold, F. & Ballou, C. E. (1957) *J. Biol. Chem.* **227**, 301–312

APPENDIX

We give here the most general rate law compatible with the following assumptions: the enzyme consists of four protomers, which can exist in four conformational states undergoing concerted transitions, each protomer in each conformational state obeys the binding scheme given in Fig. 4, and all enzyme species are in quasi-equilibrium. Owing to the quasi-equilibrium assumption, only one binding sequence leading to a given complex permits the determination of the concentration of that complex. It can thus easily be seen that only 12 dissociation constants need to be considered for each conformational state. We chose $K_{A\nu}$, $K_{AC\nu}$, $K_{ACB\nu}$, $K_{B\nu}$, $K_{C\nu}$, $K_{CB\nu}$, $K_{AB\nu}$, $K_{Q\nu}$, $K_{(CQ)\nu}$, $\bar{K}_{Q\nu}$, $\bar{K}_{C\nu}$ and $\bar{K}_{(CQ)\nu}$

($v = 1, 2, 3, 4$). We can describe the ionic strength dependence of the reaction rate by eqn. (8). For $v(\tilde{I})$, i.e. for the reaction rate at a fixed ionic strength $\tilde{I}$, one obtains the following equation by extension of the formulation of Monod *et al.* (1965):

$$v(\tilde{I}) = [E_{total}] \frac{\sum_{k=1}^{4} k_v F_v M_v G_v^3}{\sum_{k=1}^{4} M_v G_v^4}$$

where v designates the conformational state and

$$M_v = L_v \left[1 + \frac{[Mg^{2+}]}{\tilde{K}_{Cv}} + \frac{[MgATP]}{\tilde{K}_{(CQ)v}} + \frac{[ATP]}{\tilde{K}_{Qv}} \right]^4$$

(L_1 has to be set equal to 1),

$$F_v = \frac{[Pyr\text{-}P][Mg^{2+}][ADP]}{K_{Av} K_{ACv} K_{ACBv}}$$

and

$$G_v = 1 + \frac{[ADP]}{K_{Bv}} + \frac{[Mg^{2+}]}{K_{Cv}} \left(1 + \frac{[ADP]}{K_{CBv}} \right) + F_v + \frac{[Pyr\text{-}P]}{K_{Av}} \left(1 + \frac{[ADP]}{K_{ABv}} + \frac{[Mg^{2+}]}{K_{ACv}} \right) + \frac{[ATP]}{K_{Qv}} + \frac{[MgATP]}{K_{(CQ)v}}$$

$L_v = [R_v]_F / [R_1]_F$, where $[R_v]_F$ ($v = 1, 2, 3, 4$) is the concentration of the enzyme in the conformational state R_v in a ligand-free solution.

Reference

Monod, J., Wyman, J. & Changeux, J.-P. (1965) *J. Mol. Biol.* **12**, 88–118